An investigation into electron scattering from pyrazine at intermediate and high energies

A. G. Sanz, M. C. Fuss, F. Blanco, J. D. Gorfinkiel, D. Almeida, F. Ferreira da Silva, P. Limão-Vieira, M. J. Brunger, and G. García

Citation: The Journal of Chemical Physics **139**, 184310 (2013); doi: 10.1063/1.4829771
View online: http://dx.doi.org/10.1063/1.4829771
View Table of Contents: http://scitation.aip.org/content/aip/journal/jcp/139/18?ver=pdfcov
Published by the AIP Publishing

An investigation into electron scattering from pyrazine at intermediate and high energies

A. G. Sanz,[1] M. C. Fuss,[1] F. Blanco,[2] J. D. Gorfinkiel,[3] D. Almeida,[4] F. Ferreira da Silva,[4] P. Limão-Vieira,[4] M. J. Brunger,[5,6] and G. García[1,7,a)]

[1]*Instituto de Física Fundamental, Consejo Superior de Investigaciones Científicas, Serrano 113-bis, 28006 Madrid, Spain*
[2]*Departamento de Física Atómica, Molecular y Nuclear, Universidad Complutense de Madrid, Ciudad Universitaria, 28040 Madrid, Spain*
[3]*Department of Physical Sciences, The Open University, Walton Hall, Milton Keynes MK7 6AA, United Kingdom*
[4]*Laboratório de Colisões Atómicas e Moleculares, CEFITEC, Departamento de Física, Faculdade de Ciências e Tecnologia, Universidade Nova de Lisboa, 2829-516 Caparica, Portugal*
[5]*ARC Centre for Antimatter-Matter Studies, School of Chemical and Physical Sciences, Flinders University, GPO Box 2100, Adelaide, SA 5001, Australia*
[6]*Institute of Mathematical Sciences, University of Malaya, 50603 Kuala Lumpur, Malaysia*
[7]*Centre for Medical Radiation Physics, University of Wollongong, NSW 2522, Australia*

(Received 16 September 2013; accepted 28 October 2013; published online 14 November 2013)

Total electron scattering cross sections for pyrazine in the energy range 10–500 eV have been measured with a new magnetically confined electron transmission-beam apparatus. Theoretical differential and integral elastic, as well as integral inelastic, cross sections have been calculated by means of a screening-corrected form of the independent-atom representation (IAM-SCAR) from 10 to 1000 eV incident electron energies. The present experimental and theoretical total cross sections show a good level of agreement, to within 10%, in the overlapping energy range. Consistency of these results with previous calculations (i.e., the R-matrix and Schwinger Multichannel methods) and elastic scattering measurements at lower energies, below 10 eV, is also discussed. © *2013 AIP Publishing LLC*. [http://dx.doi.org/10.1063/1.4829771]

I. INTRODUCTION

Cross-section values for electron scattering over a wide energy range are important parameters in many scientific and technological applications (e.g., astrophysics, atmospheric physics, plasma physics, detector response simulations, and so on). Moreover, it is now well established that the main particles responsible for the radiation damage induced by high energy incident projectiles (electrons, protons, ions, x-rays…) are secondary electrons (SEs), which are generated along the main particle track, with an energy typically below 10 eV.[1,2] These particles, the so-called low-energy electrons (LEEs), interact with the atoms and molecules constituting biological matter to produce severe structural and chemical alterations, e.g., single- and double- strand breaks (SSBs and DSBs), in the DNA molecule.[3,4] As such, these electron induced processes have been shown to give a correct and precise description of the underlying mechanisms at the molecular level. Therefore, accurate energy deposition models should incorporate the effects of those electrons from their initial high energies down to thermal energies, e.g., though a Low Energy Particle Track Simulation (LEPTS[5]). For this reason, complete sets of interaction probabilities for electron collisions (i.e., the cross sections) over a wide energy range are needed for all the accessible scattering processes.

Although electron cross sections have been the subject of numerous experimental and theoretical studies for a great variety of molecular targets,[6,7] most of them have recently focused on the low energy region[8–11] so that those covering a wide enough energy range are available only for a few biomolecules.[12–14] Additionally, a detailed understanding of the mechanisms governing the DNA damage induced by electron collisions requires a broader knowledge of the scattering dynamics of these electrons with the constituent DNA compounds, such as the nucleobases. It is customary to employ model molecules, with simpler geometries and physicochemical properties, as this simplifies both the experimental and theoretical investigations and provides valuable information on the scattering nature and interaction probabilities. For instance, pyrimidine has been employed on various occasions as a benchmark system for the "pyrimidinic" DNA/RNA nucleobases, i.e., thymine, cytosine, and uracil. Although some simplifications can be introduced, the strongly polar nature of pyrimidine brings along additional difficulties both for the experimental and theoretical investigations. In contrast another member of the diazine group, pyrazine, provides an alternative and convenient model for the pyrimidinic bases. Pyrazine contains two nitrogen atoms at positions 1 and 4 in the six-member ring and therefore possesses a symmetric structure (see Fig. 1), giving it a non-polar nature. This characteristic is considerably advantageous: not only does it make the calculations less expensive, it also introduces less uncertainty in the measurements. In particular, as most measured elastic integral cross sections are derived from extrapolations of their differential cross sections, having a non-polar target reduces

a)Email: g.garcia@iff.csic.es

Pyrimidine Pyrazine

FIG. 1. Schematic structures of the diazine molecules pyrimidine and pyrazine.

the uncertainty in that extrapolation procedure (see later). In addition, from a fundamental perspective, pyrazine is also interesting to compare the electron interaction probabilities between it and pyrimidine, as they are structural isomers, and evaluate the effect that the permanent dipole moment of the latter has on the electron scattering dynamics.

Despite the advantages of employing pyrazine as a benchmark system, electron collisions with this target have been studied only by a few groups. Early electron transmission experiments performed by Nenner and Schulz[15] showed the formation of three low-lying π^* resonances for incident electron energies below 5 eV. The two lowest-lying resonances were identified as pure shape resonances, whereas the more energetic one, which is at around 4.1 eV, was suggested to have a mixed shape and core-excited character. Just recently, Palihawadana *et al.*[16] have measured (for the first time) absolute differential and integral elastic cross sections for electron scattering from pyrazine in the incident energy range 3–50 eV. From the theoretical point of view, Winstead and McKoy[17] calculated differential elastic cross sections in the low-energy domain by means of the Schwinger Multichannel (SMC) method,[18,19] at both the static-exchange (SE) and the static-exchange plus polarization (SEP) levels of approximation. These authors also provided strong evidence for the mixed character of the third low-lying resonance. Additionally, Mašín and Gorfinkiel[20] have reported recently a detailed analysis on low-energy electron collisions with pyrazine by means of the R-Matrix method.[21] They employed the SEP and close coupling (CC) approximation to compute elastic and electronically inelastic cross sections. Typically, a good level of accord was found between the experimental and theoretical values. However, it is worthy of note that all these investigations have been restricted to the relatively low energy domain.

It is also noteworthy that experimental total scattering cross sections for pyrazine have not previously been reported, and from the theoretical point of view that they are available only up to the ionization threshold.[20] Total cross sections are of significant general importance in scattering investigations[6,7] and are a crucial input for particle track simulations in matter, since in the latter case they are used to calculate the mean-free path between two interactions. Additionally, they serve as an essential reference value for representing the sum of all the partial, process specific, interaction integral cross sections which are typically obtained in independent measurements. This makes total scattering cross sections (TCSs) an ideal reference for checking the self-consistency of the partial cross sections. In view of this, one of the aims of this work is therefore to present reliable total electron scattering cross sections from pyrazine over the whole energy range considered here, namely 10–1000 eV. This has been measured with an experimental apparatus recently developed by Fuss *et al.*,[22] which is based on a strong axial magnetic confinement of the electron beam inside the collision chamber. This apparatus here allowed us to perform measurements for incident electron energies from 10 eV up to 500 eV. In order to provide cross sections over a broader energy range, the TCS have also been computed with a corrected form of the independent-atom model, namely the screening-corrected additivity rule (IAM-SCAR),[23,24] for electron impact energies in the range 10–1000 eV. Additionally, and over the same energy range, we also report computed integral and differential elastic cross sections for electron scattering from pyrazine, together with electronically inelastic cross sections.

The paper is organized as follows. In Sec. II, the experimental methodology and analysis techniques are described. In Sec. III, we briefly state the details of our theoretical method. In Sec. IV, we present the measured and calculated total scattering cross sections. Additionally, computed electronically inelastic cross sections together with integral and differential elastic cross sections are reported. Where possible, those results are compared to data that are available in the literature. Finally, in Sec. V, we summarize our work and present some concluding remarks from this study.

II. EXPERIMENTAL METHOD

A recently constructed[22] experimental system for measuring electron scattering cross sections, within a strong axial magnetic field, was used to perform our total cross section measurements. The functionality of this apparatus is based on the magnetic confinement of the electron beam from its entrance into the collision chamber and until its detection, so that scattered and unscattered electrons are detected together after their energy analysis. The role of the main magnetic field (0.2 T) is thus simply to translate the electron, which exhibits the exact angle and energy that resulted from a potential collision, along the central axis to the end of the collision chamber. This apparatus has been recently described in some detail,[22] therefore only a brief summary is given here.

The apparatus (a schematic diagram is given in Figure 2) consists of three regions (electron gun, collision chamber, and analyzer-detector region), connected by small orifices, which have independent magnetic fields. Electrons are generated by thermionic emission from a tungsten filament (2), and accelerated to a kinetic energy E before passing into the collision chamber (4). The magnetic field B_g of the electron gun region, oriented opposing the main field B, ensures a low angular spread of the electron beam by locally compensating for B and preventing electrons leaving the filament in oblique directions to pass through the collimators. The collision chamber itself has a geometrical length of 140 mm and is therefore sufficiently large compared to the delimiting apertures (of 1 and 2.3 mm diameter) to guarantee a well-defined region of constant pressure. Pyrazine is introduced into the system via a heated variable leak valve (6), from a steel sample-container maintained at around 40°C by means of various silicone heater mats. The chamber wall can partly absorb

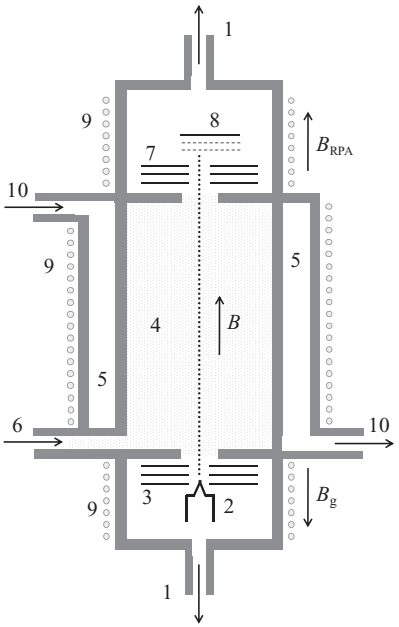

FIG. 2. Schematic diagram of the scattering apparatus: 1 — turbomolecular pumps, 2 — electron-emitting filament, 3 — extracting and accelerating electrodes, 4 — collision chamber, 5 — water jacket, 6 — gas inlet, 7 — retarding potential analyzer (RPA), 8 -- electron detector (microchannel plate assembly), 9 -- magnetic coils, and 10 — cooling liquid inlet/outlet.

the heat dissipated by the magnetic coils (9), depending on the pumping speed of the cooling liquid through the chamber's water jacket (5). Hence, the balance between solenoid current and water speed can be utilized in order to maintain a convenient chamber temperature and avoid condensation of the sample on the inner chamber walls. The pressure in the chamber is determined by an absolute capacitance manometer (MKS Baratron 627B, Germany), while the temperature is measured using a K-type thermocouple in thermal contact with the inner chamber wall. Owing to the magnetic confinement, the effective localization of the electrons after scattering (but before entering the analyzer) is within a radius of 1 mm around the central axis. After traversing the collision chamber, electrons are selected by a retarding potential analyzer (RPA) so that only those with parallel (axial) components of the kinetic energy $\geq eV_R$ (where e represents the elementary charge and V_R is the retarding potential) continue towards the detector. Note that electrons scattered backwards ($>90^\circ$) are reflected by the electron gun and traverse the collision chamber a second time before reaching the analyzer. The detector assembly is formed by two microchannel plates (Hamamatsu photonics, Japan) and an anode, and is polarized with around +2 keV. It is operated in single-pulse counting mode and connected, via some additional electronics, to a PC running a custom LabView (National Instruments) programme which registers and analyzes the signal.

Pyrazine, with a stated purity of 99%, was purchased from Sigma-Aldrich and further purified through the performance of freeze-pump-thaw cycles. Before each measurement, the energy resolution defined as $\delta E = e(V_{R,90} - V_{R,10})/2$, with $V_{R,90}$ and $V_{R,10}$ being the retarding potentials leading to 90% and 10% of transmitted electrons, was obtained from the transmission curve $I(V_R)$ in vacuum, where I is the transmitted beam intensity (electron count rate). It was generally found to be similar to the FWHM (full width at half maximum) determined from the derivatives of the transmission curves and is given, for each measurement, in Table I. Subsequently, the retarding potential was fixed to define the cut-off energy (typically passing about the 85% of the maximum beam intensity in vacuum) and then the transmitted intensity as a function of the gas pressure was recorded. For each incident electron energy, a series of 7–10 attenuation curves, each normally comprising 7–12 data pairs (pressure (p) and intensity), were then acquired. The data points were fitted by an exponential curve $I(p)$, from which the experimental total scattering cross section σ_{exp} is obtained according to the Beer-Lambert law:

$$I = I_0 e^{-nl\sigma_{exp}} = I_0 e^{-pl\sigma_{exp}/kT}. \quad (1)$$

Here, I_0 is the intensity of the non-attenuated beam (in vacuum), n is the number density of the target gas, $l = 141.3$ mm is the effective collision chamber length, k is the Boltzmann constant, and $T = \sqrt{T_c T_m}$ is the gas temperature (in K) calculated according to the thermal transpiration effect[25] between the manometer at T_m and the collision chamber at T_c. Further details on the experimental apparatus and procedures can be found in Fuss *et al.*[22]

The experimental uncertainties on the present measurements lie in the range 1.8%–5.0% (for the incident energies of this study), including the uncertainties in the determination of the collision chamber length, sample gas pressure, temperature, and incident beam energy. Furthermore, a reproducibility (standard deviation between the I(p) versus p curves of the same series) of around 2.0% (exact values are given in Table I), comprising a filament emission stability, temperature stability, (electronic) signal fluctuations, and the uncertainty in the determination of the fit function (i.e., the exponent of the attenuation curve), has been observed. Combining the aforementioned factors, one obtains a general precision of

TABLE I. Experimental total cross sections for electron collisions with pyrazine in Å^2 units. For each energy the percentage reproducibility, energy resolution (δE), angular acceptance ($\delta\theta$), and the estimated systematic error $\delta\sigma_{exp}/\sigma_{exp}$ (Eq. (5)) are specified.

E (eV)	σ_{exp} (Å^2)	Reproducibility (%)	δE (eV)	$\delta\theta$ (°)	$\delta\sigma_{exp}/\sigma_{exp}$ (%)
10	38.1	1.3	0.86	17.1	9.0
12	34.5	5.3	1.17	18.2	13.4
15	32.7	1.8	1.11	15.8	12.9
20	30.8	3.1	1.06	13.3	11.4
25	31.5	2.0	0.91	11.0	10.8
30	30.2	0.8	1.00	10.5	7.4
40	29.5	2.7	1.21	10.0	8.0
50	28.7	2.2	1.46	9.8	9.2
70	28.2	2.0	1.03	7.0	6.4
100	25.1	2.6	1.23	6.4	6.6
150	19.4	0.9	1.93	6.5	8.9
200	16.9	2.3	3.59	7.7	14.1
300	14.3	1.8	3.69	6.4	13.6
400	11.7	1.2	3.11	5.1	11.3
500	9.97	1.4	5.68	6.1	17.3

the present experimental total cross section determination of ~3.5% at incident energies ≥20 eV, and of ≲5.1% for incident energies ≤15 eV. In addition to this general uncertainty of a statistical nature, the angular acceptance $\delta\theta$ of the apparatus is a limiting aspect and represents an important source of systematic error. Due to the axial magnetic confinement, scattered electrons will pass the analyzer if the kinetic energy $E'_{\parallel}$, corresponding to the parallel component of their velocity $v'_{\parallel}$, can overcome the retarding potential V_R, i.e., $m_e v'^2_{\parallel}/2 \geq eV_R$ (where m_e is the electron mass). Hence, some elastically or rotationally inelastically scattered electrons at small-angles ($0 \leq \theta \leq \delta\theta$) or near 180° ($180-\delta\theta \leq \theta \leq 180$, for the case of backscattered and reflected electrons), can pass the potential barrier and so they do contribute to I in Eq. (1) whereas in an ideal experiment they should not. As a consequence, this fraction of the scattered electrons are not distinguished from the unscattered electrons and so will not be accounted in determining the measured cross section (σ_{exp}). Under these circumstances, σ_{exp} will always tend to be lower than the "true" value of the TCS (σ). The angular resolution in the forward direction $\delta\theta$ (angular acceptance of elastically scattered electrons during the total cross section measurements) can be calculated from the energy resolution δE, obtained from the transmission curve applying

$$\delta\theta = \sin^{-1}\sqrt{\delta E/E}. \tag{2}$$

The values of $\delta\theta$ for the present measurements were found to lie between 5.1° and 18.2°, and are listed in Table I. This means that any comparison to other total cross section data needs to take into account that the present experimental values σ_{exp} actually represents partial values,

$$\sigma_{exp}(E) \approx \sigma(E) - \sigma_{forw}(E) \quad \text{with} \tag{3}$$

$$\sigma_{forw} = 2\pi\left(\int_0^{\delta\theta} \frac{d(\sigma_{el}+\sigma_{rot})}{d}\sin\theta d\theta + \int_{180-\delta\theta}^{180} \frac{d(\sigma_{el}+\sigma_{rot})}{d}\sin\theta d\theta\right). \tag{4}$$

Note that σ_{el} and σ_{rot} denote the elastic and rotational cross sections, respectively. In general, given our energy resolution, contributions from vibrational channels to this effect are also possible. However, typically the vibrational cross section magnitudes are much smaller[7] than those of the elastic scattering process and so can be effectively ignored in this analysis. In particular for pyrazine, being a non-polar molecule, the contribution of σ_{rot} to Eq. (4) can be also ignored.

However, an estimate of the systematic error, $\delta\sigma_{exp}$(E), due to this effect, can be calculated as follows:

$$\delta\sigma_{exp}(E) \approx \frac{\sigma_{forw}(E)}{\sigma - \sigma_{forw}(E)}\sigma_{exp}(E), \tag{5}$$

where $\sigma_{forw}(E)$ and σ can be taken from the present theoretical IAM-SCAR data.

III. THEORETICAL METHOD: THE IAM-SCAR MODEL

Pyrazine cross sections in the present study have been computed by means of a corrected form of the independent-atom model (IAM), known as the screening-corrected additivity rule (SCAR) procedure. Details for this approach have been extensively given in the past.[23,24,26,27] Hence, we only summarize briefly the method here.

The basic idea of the present approach is that the molecule is not considered as a single complex target, but instead as an aggregate of individual atoms. This approximation assumes that the molecular binding does not affect the electronic distribution of the atom and therefore each atom of the molecule scatters independently from the others. In other words, the atoms of the molecule are seen as isolated entities. Thus, the first issue of this calculation is to describe the electron scattering from the atoms constituting the pyrazine molecule, namely, C, H, and N. The electron-atom interaction is represented by an *ab initio* complex optical potential: the real part accounts for the elastic scattering whereas the imaginary part represents the inelastic processes which are considered as "absorption" channels from the incident beam. The complex potential for each atom is given by:

$$\begin{aligned} V_{opt}(\mathbf{r}) &= V_R(\mathbf{r}) + iV_{abs}(\mathbf{r}) \\ &= V_s(\mathbf{r}) + V_{ex}(\mathbf{r}) + V_{pol}(\mathbf{r}) + iV_{abs}(\mathbf{r}). \end{aligned} \tag{6}$$

Here the real part comprises three terms: (i) a static term (V_s) derived from a Hartree-Fock calculation of the atomic charge distribution,[28] (ii) an exchange term (V_{ex}) which accounts for the indistinguishability of the incident and target electrons given by the semiclassical energy-dependent formula derived by Riley and Truhlar,[29] and (iii) a polarization potential (V_{pol}) that describes the long-range interactions. Our preferred potential is the one given by Zhang *et al.*,[30] which depends on the target dipole polarizability. Finally, the absorption potential (V_{abs}) is based on the quasi-free model developed by Staszewska *et al.*[31] which accounts for the electronically inelastic scattering events. Although, initially, some major discrepancies were found between results of our model and the available scattering data, they were subsequently corrected by introducing a more physical formulation of the absorption potential.[26] Further improvements to the original formulation, such as the inclusion of screening effects, local velocity corrections, and the description of the electron's indistinguishability,[27] led finally to a model capable of providing a more realistic representation of electron-atom scattering over a broad energy range. A nice example of this was provided by Zatsarinny *et al.*,[32] who showed that elastic cross sections computed with the present IAM-SCAR procedure for the atomic target iodine (I) were in very good agreement with similar cross sections calculated with the more sophisticated Dirac B-spline R-matrix (DBSR) method.

Next, cross sections for electron scattering from the molecular target pyrazine are computed from the atomic data by means of the well-known additivity rule (AR)[33,34] method. Within this approach, the molecular scattering amplitude is derived from the sum of all the relevant atomic amplitudes, including the phase coefficients, from which the molecular differential cross sections (DCSs) can be generated

subsequently. Integral cross sections (ICS) can then be determined by integrating those DCS. Total scattering cross sections (TCS) are finally derived from the sum of the elastic ICS and the absorption ICS (for all inelastic processes except vibrations and rotations). Note that a normalization procedure is introduced during the computation of the differential cross sections in order to avoid a violation of the optical theorem.[35,36] The main limitation of this procedure is that no molecular structure is considered. Hence, it is only valid for fast enough incident electrons which effectively "see" the target molecule as a sum of individual atoms, that is, for energies above ~100 eV.[27] For lower incident electron energies, the atomic cross sections are sufficiently large to overlap with each other, leading to an overestimation of the cross sections calculated with the additivity rule. In order to partially solve this limitation, Blanco and García implemented the code SCAR,[23,24] which takes into account the geometry of the molecule (atomic positions and bond lengths) by introducing some screening coefficients. Within this screening-corrected method, both the differential and integral cross sections are modified, extending the range of validity perhaps down to ~30 eV. The estimated intrinsic numerical uncertainty of the present method is within 10%.[12,13] Note that our SCAR method has been shown on numerous occasions to be a powerful tool to calculate electron scattering cross sections, for a large variety of molecules,[37–39] from intermediate up to high energies.

Regarding the present calculations, note that the corresponding atomic cross sections for C, H, and N have been calculated and discussed in the past.[27] Finally note that the geometrical parameters required to calculate the molecular cross sections for pyrazine have been taken from Innes *et al.*[40]

IV. RESULTS

A. Total and integral cross sections

The present experimental total cross sections (TCS) for electron scattering from pyrazine are plotted in Fig. 3, together with theoretical TCS computed with the IAM-SCAR method. Further, these experimental and theoretical TCS are listed in Tables I and II, respectively. It can be seen that our experiment and theory results show a general agreement, to within 11%–25%, over the whole energy range where the measurements were performed, i.e., 10–500 eV. Note, however, that the experimental values are dependent on the angular restrictions, since the experimental apparatus does not perfectly discriminate against elastically and rotationally scattered electrons to the forward and backward angles, as was explained in Sec. II. This means that the experimental TCS effectively neglects the elastic and rotational excitation contribution of the lowest and highest scattering angles, and so is a lower bound on the true TCS values. In order to provide a more realistic comparison, the IAM-SCAR cross sections for σ-σ_{forw} have been computed according to Eqs. (3) and (4) in an attempt to mimic the experimental conditions (see Table I). As is appreciated in Fig. 3, the level of accord between the experimental TCS and the IAM-SCAR CS for σ-σ_{forw} markedly improves in the lower energy region and became excellent

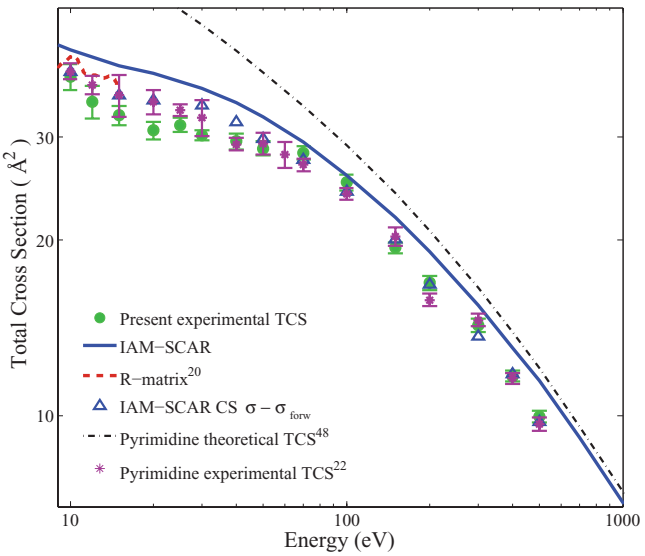

FIG. 3. Present total cross section for electron scattering by pyrazine: experimental TCS (full green circles), IAM-SCAR calculations (solid blue line), and the IAM-SCAR CS for $\sigma - \sigma_{\text{forw}}$ (blue up-triangle). Also shown are the results from the R-matrix theory (dashed red line).[20] For comparison, the pyrimidine total CS, both theoretical (dashed-dotted black line; see Sanz *et al.*[48]) and experimental[22] (purple asterisks) are additionally plotted.

with increasing energies (above ~ 70 eV). Note that due to the dependence of $\delta\theta$ on the relative value $\delta E/E$, the angular acceptance of the experimental configuration decreased with increasing energy, from 17.1° at 10 eV down to 6.1° at 500 eV. This means that at higher energies it is possible to better discriminate against forward and backward scattered electrons, introducing therefore less uncertainty in the measurements. Our present theoretical and experimental data are also compared with previous total cross sections computed with the R-matrix method by Mašín and Gorfinkiel.[20] Their data are given as a combination of the most physical results they obtained, i.e., the SEP model,[20] using the diffuse

TABLE II. Present theoretical elastic, electronically inelastic (electronic-state excitation and ionization), and total integral cross sections for electron scattering from pyrazine in the energy range from 10 to 1000 eV.

Energy (eV)	Elastic (Å^2)	Electronic inelastic (Å^2)	Total (Å^2)
10	42.28	0.10	42.38
15	36.96	2.88	39.84
20	31.36	7.31	38.67
30	24.16	12.35	36.51
40	20.55	13.86	34.41
50	18.20	14.25	32.45
70	15.18	14.14	29.32
100	12.52	13.30	25.82
150	10.08	11.76	21.84
200	8.62	10.50	19.12
300	6.83	8.68	15.51
400	5.71	7.42	13.13
500	4.96	6.52	11.48
700	3.95	5.24	9.18
1000	3.02	4.06	7.08

basis set 6-311+G**, for energies below the first electronic excitation state (∼4eV[41]) and the CC approximation,[20] with the compact basis set cc-pVDZ, for energies above this threshold. The latter approximation accounts for the electronic excitations; however, ionization is missing from the calculations since this would have required the inclusion of pseudostates which drastically increases the computational cost. The R-matrix cross sections are therefore believed to be accurate below the ionization threshold (∼9.4 eV[42]), whereas for higher energies they are considered merely indicative and tend to be somewhat underestimated in magnitude. It can be observed in Fig. 3 that the R-matrix[20] results are in pretty good agreement with the present IAM-SCAR calculations at incident electron energies where a comparison is possible, although as expected they tend to be slightly smaller in magnitude due to the omission of the ionization states.

In this plot (Fig. 3) are also shown for comparison TCS for electron scattering from pyrimidine. It is interesting to compare the response of both molecules to electron collisions, since they are structural isomers (see Fig. 1) and therefore have similar physico-chemical properties, such as the polarizibility ($\alpha \sim 59.3$ and $\alpha \sim 60$ a.u. for pyrimidine[43,44] and pyrazine,[45] respectively). However, the high symmetry of pyrazine implies that this molecule has no permanent dipole moment, whereas the shift in position of one of the nitrogen atoms in pyrimidine confers to this molecule a strong polar nature ($\mu \sim 2.334$[46]). In Fig. 3, we therefore include the experimental pyrimidine TCS measured recently by Fuss *et al.*[22] and the recommended theoretical TCS, obtained by means of combining the R-matrix cross sections calculated by Mašín *et al.*[47] and some IAM-SCAR results, as has been explained in Sanz *et al.*[48] According to the latter work, e^--pyrimidine cross sections are accurately given by the R-matrix approach[47] for energies below the ionization threshold (located at 9.7 eV for pyrimidine[49]), which is in turn given as a combination of the SEP and CC approximations for energies below and above the first electronic excitation state, respectively. Whereas for energies above the ionization threshold, cross sections computed with the IAM-SCAR procedure are preferred.[48] It can be seen that the magnitudes of the experimental pyrimidine TCS are comparable to those for the present experimental TCS for pyrazine, to within the experimental uncertainty, and that both TCS display a similar energy dependence. A logical initial inference from this observation is that the permanent dipole moment of pyrimidine is having only a small effect on its scattering dynamics. In contrast, important differences are found on the theoretical TCS data between the pyrimidine and pyrazine results, in particular at the lower energies. It is known that the strongly polar nature of the pyrimidine molecule causes significant dipole-induced rotational excitations, especially at low incident energies and in the forward direction. Whereas these angles are not accessible for all scattering processes in the experimental configuration, they constitute an important contribution for the theoretical TCS. In contrast, non-polar molecules such as pyrazine are not as affected by angular discrimination limitations in the apparatus. This is why the theoretical pyrimidine cross sections are considerably larger than those of pyrazine. As the same behaviour is not observed between the experimental pyrimidine and pyrazine TCS data, we can understand this as being essentially due to the experimental angular acceptance which effectively ignores part of the small angle distribution where the dipole effects are more important.

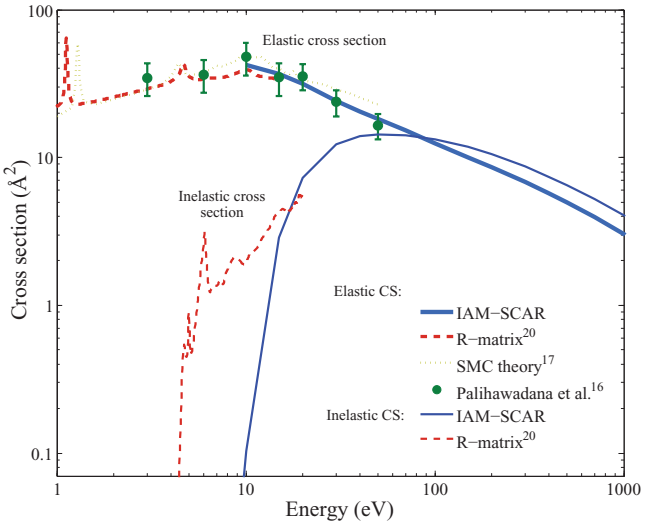

FIG. 4. Present computed integral elastic cross section for electron scattering by pyrazine with the IAM-SCAR method (solid blue line). Also shown are the elastic ICS computed with the R-matrix method (dashed red line)[20] and the SMC theory (dotted green line),[17] and the experimental measurements provided by Palihawadana *et al.*[16] (full green circles). In addition the present IAM-SCAR electronically inelastic integral cross sections are shown, together with those correspondingly calculated with the R-matrix[20] method.

The present integral elastic and inelastic cross sections computed with the IAM-SCAR method, in the energy range 10–1000 eV, are shown in Fig. 4 and listed in Table II. At the common energies of overlap, we find excellent agreement between the present calculations and previous integral elastic cross sections computed with the R-matrix approach.[20] Note, in fact, that both curves merge at around 15 eV. Also, fairly good agreement is found with earlier Schwinger multichannel calculations (SMC) performed by Winstead and McKoy[17] in the 10–20 eV energy range. In addition, there is a very good level of accord between our present calculations and the measurements from Palihawadana *et al.*[16] for the energy range where such a comparison is possible. It is worthy of note that their experimental DCS measurements were conducted in a limited angular range, so that their integral elastic cross sections have been derived by extrapolating the measurements to 0° and 180° following the shape of the corresponding SMC angular distribution at each energy. However, at energies above 20 eV, the SMC procedure somewhat overestimates the experimental values, whereas the IAM-SCAR results lies within the experimental uncertainty bars. It should also be noted that both the R-matrix[20] and SMC[17] methods indicate significant low energy resonance structure in their elastic ICS. Such resonance enhancements cannot be predicted by our IAM-SCAR approach, due to its underlying construction, so that both the aforementioned methods are invaluable at the lower energies.

Regarding the electronically inelastic cross sections, they were calculated through the $V_{abs}(r)$ absorption term of the

IAM-SCAR optical potential. In contrast to the R-matrix method, the IAM-SCAR approach does account for the ionization process. Although the first electronic excitation state of pyrazine has been placed at around ∼4.0 eV,[41] the IAM-SCAR onset for the inelastic events occurs at ∼10 eV, followed by a noticeable rise of the summed inelastic ICS for increasing energies (see Fig. 4). The fact that electronically excited states lying below 10 eV are underestimated in our IAM-SCAR approach reflects the intrinsic limitations of the present independent-atom model in the low-energy region. Note, however, that both the R-matrix and IAM-SCAR inelastic ICS became in good agreement at around 18 eV. Additionally, it should also be noted that processes involving nuclear motion, i.e., rotational and vibrational excitations, have not been considered in the theoretical component of this study. Nevertheless, this restriction is not thought to be significant due to the non-polar nature of the present target molecule.

B. Differential cross sections

The present calculated elastic differential cross sections for pyrazine are plotted in Fig. 5, at some selected incident electron energy values. It can be seen that at the lower energies there is quite good agreement between the elastic DCS computed with the R-matrix[20] and SMC[17] approaches and the experimental data provided by Palihawadana *et al.*,[16]

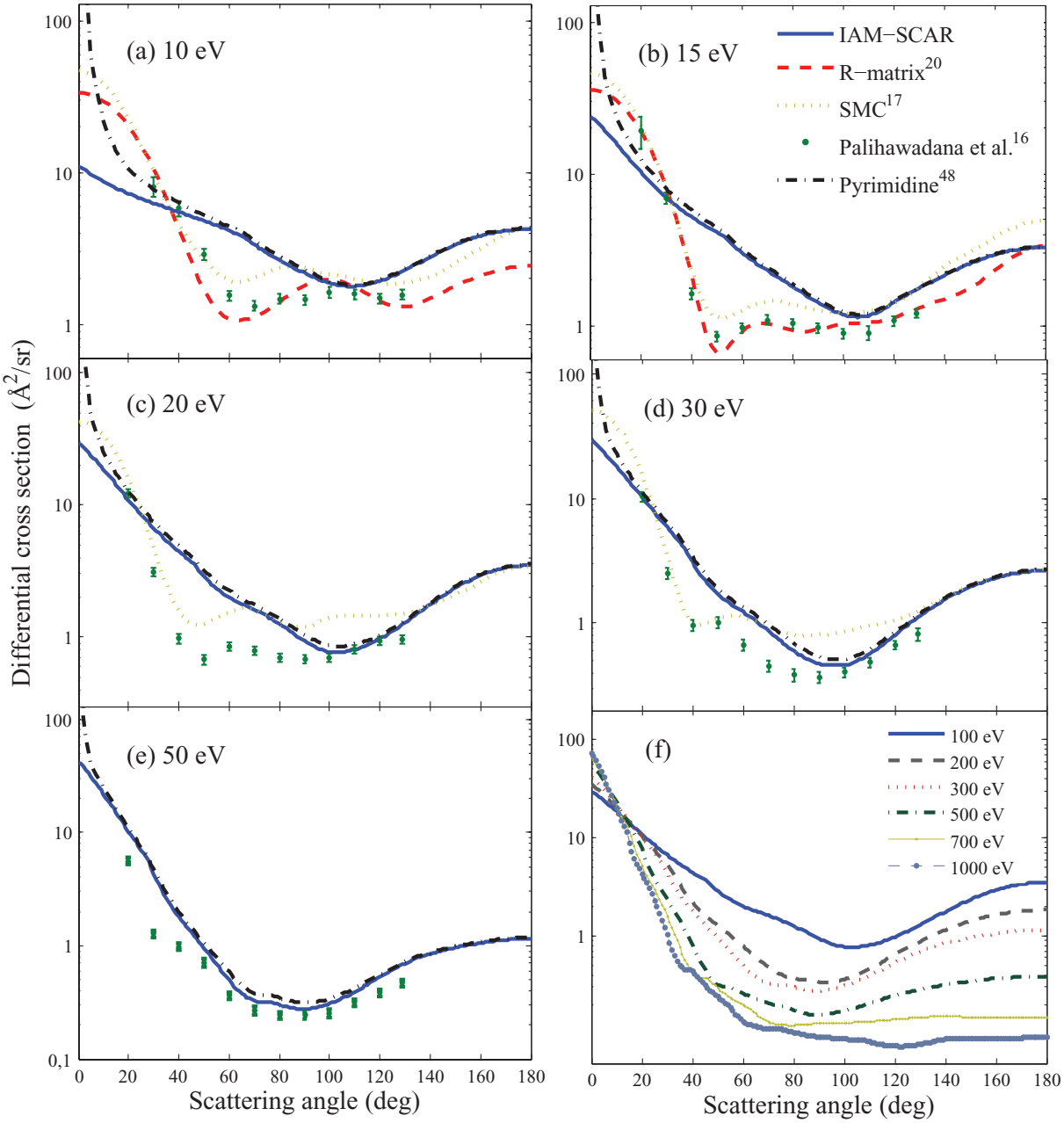

FIG. 5. Elastic differential cross sections for electron scattering from pyrazine for the incident energies indicated in the panels. (a)–(e): The present IAM-SCAR calculations (solid blue line), the R-matrix theory (dashed red line),[20] the SMC calculations (dotted green line),[17] and experimental measurements provided by Palihawadana *et al.*[16] (full green circles) are shown. Theoretical pyrimidine elastic DCSs (dashed-dotted black line; see Refs. 47 and 48) are also given. (h) shows the angular distributions computed with our IAM-SCAR model from 100 eV up to 1000 eV.

in particular at 10 and 15 eV incident electron energy (see Figs. 5(a) and 5(b), respectively). At these energies, the elastic differential cross sections computed with the IAM-SCAR approach fail to reproduce the shape of the experimental angular distribution. As mentioned above, we do not expect the IAM-SCAR procedure to be accurate below about 20 eV, and the discrepancies observed are therefore a consequence of the intrinsic limitation of this method at low energies. However, as the energy increases up to 50 eV, the independent-atom model results come into better agreement with the experimental data from Palihawadana *et al.*[16] at scattering angles above 40°. Note that the angular dependence obtained in the experimental DCSs is characterized by a shoulder at around 50°–60°, and a broad minimum at around 120° at 10 eV, which is progressively shifted to lower angles as the impact energy increases (it is around 80° at 50 eV). The IAM-SCAR approach also shows this broad minimum around 90°–110° at 10 eV, which becomes less pronounced with increasing energies and tends finally to disappear (see Fig. 5(f)). However, our method fails to reproduce the low-lying shoulder. This result is not unexpected, since similar behaviour was found in earlier studies[50] with benzene and pyrimidine. The experimental elastic angular distributions of these targets[36,51] are also characterized by the presence of a shoulder around 40°, which our IAM-SCAR theory fails to predict. In addition, for energies below 100 eV, the benzene and pyrimidine IAM-SCAR cross sections always lie above the measurements in the angular range 10°–50°, such as we observe here for pyrazine. In contrast, very good agreement was found in benzene and pyrimidine with the experimental data at larger scattering angles than 50°, which is also consistent with what we observe here for pyrazine. Moreover, for energies above 100 eV, the lower energy discrepancies in benzene and pyrimidine disappear, and an excellent agreement was found in the entire angular range.[36,48,51] Unfortunately, for pyrazine, there are no further experimental data available in the literature for electron collisions at energies higher than 50 eV. Given the similarities among the three molecules, both in structure and physico-chemical properties, it is reasonable to expect the pyrazine IAM-SCAR results to be accurate for $\theta > 50°$ in the energy range 50–100 eV, and in the entire angular range for energies above 100 eV (Fig. 5(h)).

For comparison, we have also plotted in Fig. 5 the theoretical angular distribution curves for electron scattering from pyrimidine[47,48]as calculated with our IAM-SCAR method. In general, similar behaviour is found in the DCS results from both species for angles larger than 20°; however, noticeable differences arise at angles less than 20° where the pyrimidine elastic DCS results tend to be significantly larger in magnitude. As mentioned before, this latter behaviour is attributed to the strong dipole interaction that dominates the scattering dynamics in the forward direction, in particular at low electron impact energies.

Finally, we comment on the apparent paradox between the very good agreement between the data of Palihawadana *et al.*[16] and our IAM-SCAR results for the elastic ICS, over the common energy range, and the lesser level of accuracy at the DCS level. Quite simply, this results (with the help of the sin θ weighting factor in calculating the ICS from the DCS) due to a serendipitous cancellation in the effect of having different theoretical and experimental DCS contributions to the integrand of the ICS. Thus the agreement at the elastic CS level should be considered to be little fortuitous.

V. CONCLUSIONS

In this study, we have presented absolute total cross sections (TCS) for electron scattering from pyrazine, as measured with a recently built apparatus.[22] Those measurements were performed for incident electron energies between 10 and 500 eV. In order to cover a wider energy range, TCS have also been computed with the IAM-SCAR method from 10 to 1000 eV. We have obtained quite good agreement between our experimental and theoretical results at energies where a comparison is possible, as well as with previous cross sections computed with the R-matrix method.[20] Due to the angular acceptance in the experimental measurements, there is a range of angles for which elastic and rotational collisions are not discriminated against. Therefore, in order to compare "like with like," theoretical cross sections for $\sigma - \sigma_{\text{forw}}$, emulating the experimental conditions, have also been calculated. These cross sections have been shown to be in even better agreement with the experimental values. Integral and differential elastic as well as integral inelastic cross sections were also computed with the IAM-SCAR approach. Agreement with the previous R-matrix[20] and the SMC[17] results, at energies below 20 eV, was generally very good for the elastic ICS. Agreement with corresponding measured data from Palihawadana *et al.*[16] was excellent across the entire common energy range. The level of agreement at the elastic DCS level, with the SMC,[17] R-matrix,[20] and measured data[16] was less satisfactory, although as expected it improved with increasing energy.

Finally, a comparison of the present theoretical e^--pyrazine differential cross sections with our previous calculation on scattering from pyrimidine showed in general a good level of accord, both in shape and magnitude, for angles larger than 20°. However, in the forward direction, the pyrimidine cross sections rise dramatically in magnitude due to the dominant effect of the dipole interaction at small angles and in particular at low incident electron energies. This behaviour is also reflected in the total and integral elastic cross sections, provoking significantly larger theoretical TCS. On the other hand, in the experimental TCS data this effect is not observed to the same extent, due to the finite angular resolution of the experimental-apparatus in the forward direction. This study shows the efficacy of combining experimental and theoretical approaches, in order to provide reliable and comprehensive scattering cross sections for colleagues wishing to model, for example, charged particle tracks in molecules of medical and biological importance.

ACKNOWLEDGMENTS

This work is partially supported by the Spanish Ministerio de Economía y Competitividad (Projects FIS2009-10245 and FIS2012-31320) and the EU/ESF COST Action MP1002 "Nanoscale Insights into Ion Beam Cancer Therapy (Nano-IBCT)". M.C.F. is financially supported by

the Comunidad Autónoma de Madrid local government. This work was also supported by the EPSRC and the Australian Research Council through its Centres of Excellence programme. We acknowledge Professor Carl Winstead for providing us with numerical values of their data presented in this paper. D.A. and F.F.S. acknowledge the Portuguese Foundation for Science and Technology (FCT-MEC) for a post-graduate SFRH/BD/61645/2009 and post-doctoral SFRH/BPD/68979/2010 grants. We are also grateful to the partial funding from the Portuguese research Grant Nos. PEst-OE/FIS/UI0068/2011 and PTDC/FIS-ATO/1832/2012 through FCT-MEC. P.L.-V. acknowledges his visiting Professor position at The Open University, UK.

[1]International Commission on Radiation Units and Measurements, ICRU Report 31 (ICRU, Washington, DC, 1979).
[2]S. M. Pimblott and J. A. La Verne, Radiat. Phys. Chem. **76**, 1244 (2007).
[3]B. Boudaiffa, P. Cloutier, D. Hunting, M. A. Huels, and L. Sanche, Science **287**, 1658 (2000).
[4]Z. Cai, P. Cloutier, D. Hunting, and L. Sanche, J. Phys. Chem. B **109**, 4796 (2005).
[5]A. Muñoz, J. M. Perez, G. Garcia, and F. Blanco, Nucl. Instrum. Methods Phys. Res. A **536**, 176 (2005).
[6]S. Trajmar, D. F. Register, and A. Chutjian, Phys. Rep. **97**, 219 (1983).
[7]M. J. Brunger and S. J. Buckman, Phys. Rep. **357**, 215 (2002).
[8]R. J. Gulley, S. L. Lunt, J. P. Ziesel, and D. Field, J. Phys. B **31**, 2735 (1998).
[9]A. Faure, J. D. Gorfinkiel, and J. Tennyson, J. Phys. B **37**, 801 (2004).
[10]F. A. Gianturco and R. R. Lucchese, J. Chem. Phys. **114**, 3429 (2001).
[11]M. Rezaee, P. Cloutier, A. D. Bass, M. Michaud, D. J. Hunting, and L. Sanche, Phys. Rev. E **86**, 031913 (2012).
[12]M. C. Fuss, A. Muñoz, J. C. Oller, F. Blanco, M. J. Hubin-Franskin, D. Almeida, P. Limão-Vieira, and G. García, Chem. Phys. Lett. **486**, 110 (2010).
[13]A. Muñoz, J. C. Oller, F. Blanco, J. D. Gorfinkiel, P. Limão-Vieira, and G. García, Phys. Rev. A **76**, 052707 (2007).
[14]A. G. Sanz, M. C. Fuss, F. Blanco, F. Sebastianelli, F. A. Gianturco, and G. García, J. Chem. Phys. **137**, 124103 (2012).
[15]I. Nenner and G. J. Schulz, J. Chem. Phys. **62**, 1747 (1975).
[16]P. Palihawadana, J. P. Sullivan, S. J. Buckman, and M. J. Brunger, J. Chem. Phys. **137**, 204307 (2012).
[17]C. Winstead and V. McKoy, Phys. Rev. A **76**, 012712 (2007).
[18]K. Takatsuka and V. McKoy, Phys. Rev. A **24**, 2473 (1981).
[19]K. Takatsuka and V. McKoy, Phys. Rev. A **30**, 1734 (1984).
[20]Z. Mašín and J. D. Gorfinkiel, J. Chem. Phys. **135**, 144308 (2011).
[21]P. G. Burke, *R-Matrix Theory of Atomic Collisions: Application to Atomic, Molecular and Optical Processes* (Springer, 2011).
[22]M. C. Fuss, A. G. Sanz, F. Blanco, J. C. Oller, P. Limão-Vieira, M. J. Brunger, and G. García, Phys. Rev. A **88**, 042702 (2013).
[23]F. Blanco and G. Garcia, Phys. Lett. A **317**, 458 (2003).
[24]F. Blanco and G. Garcia, Phys. Lett. A **330**, 230 (2004).
[25]M. Knudsen, Ann. Phys. **336**, 205 (1909).
[26]F. Blanco and G. Garcia, Phys. Lett. A **295**, 178 (2002).
[27]F. Blanco and G. García, Phys. Rev. A **67**, 022701 (2003).
[28]R. D. Cowan, *The Theory of Atomic Structure and Spectra* (University of California Press, London, 1981).
[29]M. E. Riley and D. G. Truhlar, J. Chem. Phys. **63**, 2182 (1975).
[30]X. Z. Zhang, J. F. Sun, and Y. F. Liu, J. Phys. B **25**, 1893 (1992).
[31]G. Staszewska, D. W. Schwenke, D. Thirumalai, and D. G. Truhlar, Phys. Rev. A **28**, 2740 (1983).
[32]O. Zatsarinny, K. Bartschat, G. Garcia, F. Blanco, L. R. Hargreaves, D. B. Jones, R. Murrie, J. R. Brunton, M. J. Brunger, M. Hoshino, and S. J. Buckman, Phys. Rev. A **83**, 042702 (2011).
[33]J. W. Otvos and D. P. Stevenson, J. Am. Chem. Soc. **78**, 546 (1956).
[34]Y. Jiang, J. Sun, and L. Wan, Phys. Rev. A **52**, 398 (1995).
[35]A. R. Milosavljević, F. Blanco, J. B. Maljković, D. Šević, G. García, and B. P. Marinković, New J. Phys. **10**, 103005 (2008).
[36]J. B. Maljković, A. R. Milosavljević, F. Blanco, D. Šević, G. García, and B. P. Marinković, Phys. Rev. A **79**, 052706 (2009).
[37]P. Limão-Vieira, F. Blanco, J. C. Oller, A. Muñoz, J. M. Pérez, M. Vinodkumar, G. García, and N. J. Mason, Phys. Rev. A **71**, 032720 (2005).
[38]H. Kato, A. Suga, M. Hoshino, F. Blanco, G. García, P. Limão-Vieira, M. J. Brunger, and H. Tanaka, J. Chem. Phys. **136**, 134313 (2012).
[39]M. C. Fuss, A. G. Sanz, A. Muñoz, T. P. D. Do, K. Nixon, M. J. Brunger, M. J. Hubin-Franskin, J. C. Oller, F. Blanco, and G. García, Chem. Phys. Lett. **560**, 22 (2013).
[40]K. K. Innes, I. G. Ross, and W. R. Moomaw, J. Mol. Spectrosc. **132**, 492 (1988).
[41]P. Weber and J. Reimers, J. Phys. Chem. A **103**, 9821 (1999).
[42]D. M. P. Holland, A. W. Potts, L. Karlsson, M. Stener, and P. Decleva, Chem. Phys. **390**, 25 (2011).
[43]C. Hattig, O. Christiansen, S. Coriani, and P. Jorgensen, J. Chem. Phys. **109**, 9237 (1998).
[44]B. Jansik, D. Jonsson, P. Salek, and H. Agren, J. Chem. Phys. **121**, 7595 (2004).
[45]See http://cccbdb.nist.gov/ for experimental and computational thermochemical data for gas-phase atoms and molecules.
[46]G. L. Blackman, R. D. Brown, and F. R. Burden, J. Mol. Spectrosc. **35**, 444 (1970).
[47]Z. Mašín, J. D. Gorfinkiel, D. B. Jones, S. M. Bellm, and M. J. Brunger, J. Chem. Phys. **136**, 144310 (2012).
[48]A. G. Sanz, M. C. Fuss, F. Blanco, Z. Mašín, J. D. Gorfinkiel, F. Carelli, F. Sebastianelli, F. A. Gianturco, and G. García, "Electron scattering cross section calculations for polar molecules over a broad energy range," Appl. Radiat. Isot. (in press).
[49]N. Hush and A. S. Cheung, Chem. Phys. Lett. **34**, 11 (1975).
[50]D. B. Jones, S. M. Bellm, P. Limão-Vieira, and M. J. Brunger, Chem. Phys. Lett. **535**, 30 (2012).
[51]H. Kato, M. C. Garcia, T. Asahina, M. Hoshino, C. Makochekanwa, and H. Tanaka, Phys. Rev. A **79**, 62703 (2009).